Asociación Argentina
de Mecánica Computacional

Mecánica Computacional Vol XXXII, págs. 913-926 (artículo completo)
Carlos G. García Garino, Aníbal E. Mirasso, Mario A. Storti, Miguel E. Tornello (Eds.)
Mendoza, Argentina, 19-22 Noviembre 2013

NON-LINEAR DYNAMIC ANALYSIS OF REINFORCED CONCRETE SHELLS UNDER SEISMIC LOAD

Jorge Palomino Tamayo[a], **Armado M. Awruch**[b] **e Inácio Benvegnu Morsch**[b]

[a]*CEMACOM, Computational Mechanical Center, Engineering School, Federal University of Rio Grande do Sul, Av. Osvaldo Aranha, 99-3º Andar, 90035-190, Porto Alegre, RS, Brazil, lpt.jorge@gmail.com, http://www.ppgec.ufrgs.br/cemacom/*

[b]*PPGEC, Department of Civil Engineering, Engineering School, Federal University of Rio Grande do Sul, Av. Osvaldo Aranha, 99-3º Andar, 90035-190, Porto Alegre, RS, Brazil, morsch@ufrgs.br, awruch@ufrgs.br http://www6.ufrgs.br/engcivil/ppgec/*

Key words: Reinforced concrete, Seismic load, Finite elements.

Abstract. Details of a finite element non-linear dynamic analysis on a reinforced concrete (RC) containment shell of a nuclear power plant subjected to seismic load is presented in this work. A three-dimensional (3D) 20-noded brick finite element is used for spatial discretisation. The concrete in compression is modeled using a modified Drücker-Prager elasto-plastic constitutive law. This constitutive law includes the strain rate sensitive effect, which is considered to be suitable for transient loading. Cracking of concrete is modeled by using a smeared approach and the tension-stiffening effect is considered by a strain-softening rule. A model based on fracture mechanics, using the concept of constant fracture energy release, is used to relate the strain softening effect to the element size in order to guaranty mesh independency in the numerical prediction. The reinforcement is also represented by a smeared approach and a classical elasto-plastic material model is adopted for reinforcing steel bars. Finally, results obtained with the present numerical model are compared with those obtained by other authors in terms of time history of displacements and cracking patterns.

1 INTRODUCTION

Containment shells are one important component of nuclear power plants and are normally constructed from reinforced concrete (RC). Because these structures are necessary for the production of nuclear energy, special consideration must be taken in their analysis and design. These aspects are more relevant when seismic actions may occur in the region where the nuclear power plant was built. While these structures are invariably designed to remain elastic under normal service conditions, they may suffer distress under the action of unforeseen extreme loads (Manjuprasad et al., 2001). In this work, a numerical model based on the finite element method is presented for the analysis of RC shells under seismic actions. In this work 20-noded brick finite elements are used to model the concrete where the reinforcing steel bars are considered to be smeared within each element and represented by membrane elements as shown in Figure 1. Concrete cracking, nonlinearity of concrete in compression, yielding of the steel bars in tension and compression and strain rate effects are considered properly in the present constitutive model. The numerical model has been validated in other works (see e.g. Tamayo et al., 2013), but seismic actions were not considered. Then, validation is done by comparing present results with those obtained by Liu (1985) in the case of time history of displacements and also with those obtained in Cervera et al. (1988) in relation to cracking patterns for different time steps.

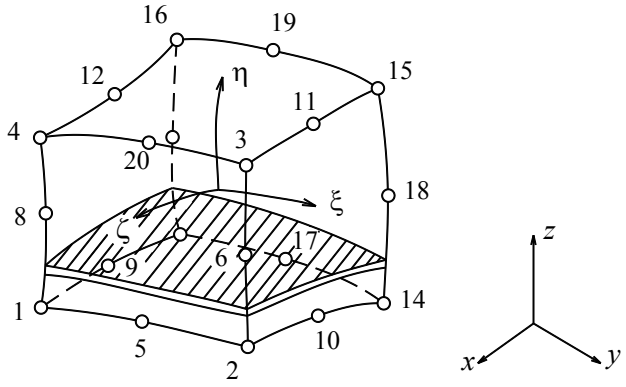

Figure 1: Local system: 20-noded brick element

2 FINITE ELEMENT FORMULATION

2.1 Finite element formulation and constitutive model of the 3D brick element

The 20-node isoparametric quadratic brick element is used here to represent the concrete shell structure where the reinforcement bars are modeled using the smeared layer approach. The displacement field within the element is defined in terms of the shape functions and displacement values at the nodes. Each nodal point has three degrees of freedom u, v and w along the cartersian coordinates x, y and z, respectively. Therefore, for each element the displacement vector is expressed in the following manner:

$$\{U\}_b = \{u_1, v_1, w_1, u_2, v_2, w_2 \ldots\ldots\ldots u_{20}, v_{20}, w_{20}\}. \tag{1}$$

The strain components vector, in terms of displacement components, is defined by:

$$\{\varepsilon\}=\begin{Bmatrix}\varepsilon_x\\ \varepsilon_y\\ \varepsilon_z\\ \gamma_{xy}\\ \gamma_{yz}\\ \gamma_{xz}\end{Bmatrix}=\sum_{k=1}^{20}\begin{bmatrix}\frac{\partial N_k}{\partial x} & 0 & 0 & \frac{\partial N_k}{\partial y} & 0 & \frac{\partial N_k}{\partial x}\\ 0 & \frac{\partial N_k}{\partial y} & 0 & \frac{\partial N_k}{\partial x} & \frac{\partial N_k}{\partial z} & 0\\ 0 & 0 & \frac{\partial N_k}{\partial z} & 0 & \frac{\partial N_k}{\partial y} & \frac{\partial N_k}{\partial z}\end{bmatrix}^T\begin{Bmatrix}u_i\\ v_i\\ w_i\end{Bmatrix} \tag{2}$$

or

$$\{\varepsilon\}_b=[B]_b\{U\}_b\,. \tag{3}$$

where N_k is the shape function of node k and $[B]_b$ is the usual strain-displacement matrix. The stress and strain components are related by the following expression:

$$\{\sigma\}_b=\begin{bmatrix}\sigma_x & \sigma_y & \sigma_z & \tau_{xy} & \tau_{yz} & \tau_{xz}\end{bmatrix}^T=[D]\{\varepsilon\}_b\,. \tag{4}$$

where $[D]$ is the material constitutive matrix in the global system. Equivalent nodal forces, at a given iteration i, are expressed in the following manner:

$$\{P\}_b^i=\int_V[B]_b^T\{\sigma\}_b^i\,dV \tag{5}$$

The stiffness matrix for a concrete element of volume V can be expressed as:

$$[K]_b^i=\int_V[B]_b^T[D]_{et}^i[B]_b\,dV \tag{6}$$

where $[D]_{et}^i$ is the uncracked, cracked or elasto-plastic constitutive matrix for the concrete material and the elastic or elasto-plastic constitutive matrix for the steel reinforcement. A reduced integration rule of 8 points is found to be suitable to diminish shear locking effect. Concrete in compression is modeled using the associated theory of plasticity; a modified Drucker-Prager yield criterion (see Figure 2a), which was proposed by Cervera et al. [1], is used in this work. Due to nonlinear hardening behavior, this yield criterion defines an initial yield surface at an effective stress equal to $\sigma_0=0.3\,f_c$ (which is the beginning of the plastic deformation) and a limit surface separating a nonlinear state from a perfect elasto-plastic one, as it is shown in Figure 2b. The yield criterion is defined as:

$$F(\sigma)=cI_1+\left\{c^2I_1^2+3mJ_2\right\}^{1/2}=\sigma_o(\bar{\varepsilon}_p) \tag{7}$$

where I_1 and J_2 are the first and the deviatoric second stress invariants, respectively. In addition, σ_0 is the effective stress which depends on the effective plastic deformation $\bar{\varepsilon}_p$, being this last parameter defined in terms of the plastic work developed by the material. The constants c and m are evaluated from experimental test and are equal to 0.1775 and 1.355, respectively. The associated flow rule is defined as:

$$d\varepsilon_{ij}^p=d\lambda\frac{\partial F(\sigma)}{\partial\sigma_{ij}}=\frac{\{g\}^T[D]_e}{H'+\{g\}^T[D]_e\{g\}}\{d\varepsilon\}\frac{\partial F(\sigma)}{\partial\sigma_{ij}} \tag{8}$$

with the flow vector given by:

$$\{g\}^T = \left[\frac{\partial F}{\partial \sigma_x} \quad \frac{\partial F}{\partial \sigma_y} \quad \frac{\partial F}{\partial \sigma_{xy}} \quad \frac{\partial F}{\partial \sigma_{xz}} \quad \frac{\partial F}{\partial \sigma_{yz}} \right] \tag{9}$$

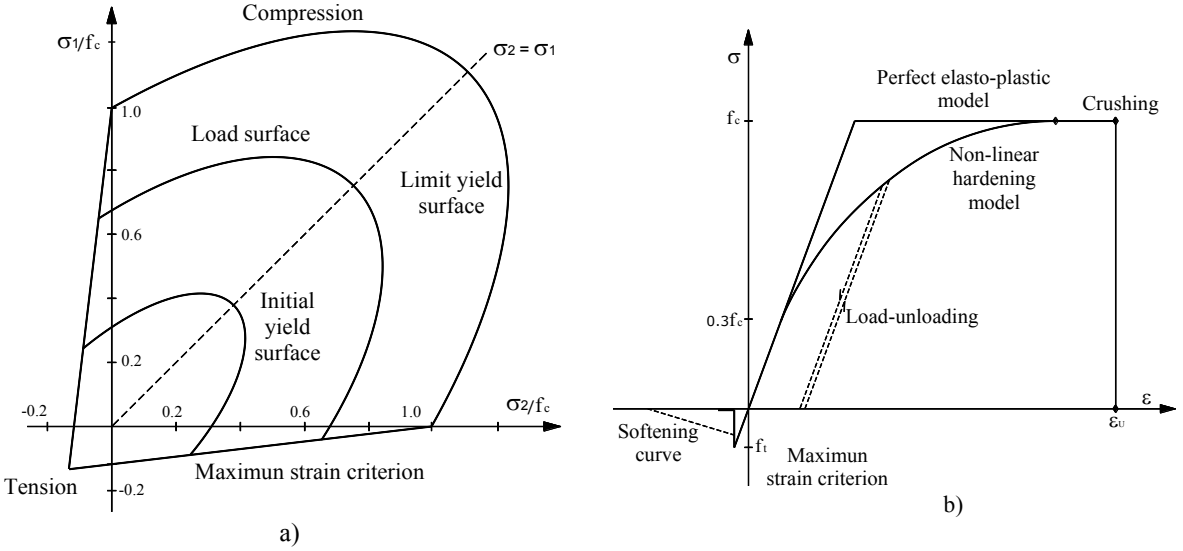

Figure 2: a) Bi-axial representation of constitutive model for concrete b) Uni-axial representation of constitutive model for concrete

In Equation (8), $\{d\varepsilon\}$ contains the components of the total strain, $d\varepsilon_{ij}^p$ is a component of the plastic strain tensor, $[D]_e$ is the elastic constitutive matrix and H' is the hardening parameter established as the slope of the one-dimensional curve which defines the hardening rule. This curve known as "Madrid parabola" is defined by the following expression:

$$\sigma_y = H(\bar{\varepsilon}_p) = E_c \bar{\varepsilon}_p + \left(2E_c^2 \varepsilon_o \bar{\varepsilon}_p\right)^{1/2} \tag{10}$$

where E_c is the elastic modulus, ε_o represents the total strain at maximum compression stress f_c. The elasto-plastic constitutive relation is expressed in the following differential form:

$$\{d\sigma\} = [D]_{et}\{d\varepsilon\} = \left\{ [D]_e - \frac{[D]_e \{g\}\{g\}^T [D]_e}{H' + \{g\}^T [D]_e \{g\}} \right\} \{d\varepsilon\} \tag{11}$$

where $[D]_{et}$ is the elasto-plastic constitutive matrix. Finally, the crushing condition is given by:

$$cI_1' + \left\{c^2 I_1'^2 + 3mJ_2'\right\}^{1/2} = \varepsilon_u \tag{12}$$

where I_1' and J_2' are the first and the deviatoric second strain invariants, respectively and ε_u represents the ultimate deformation extrapolated from experimental test (it is taken here as 0.0035). Earlier developments and studies suggest that a concrete model intended for transient

analysis should be rate and history dependent. To describe rate effects, the constitutive law, which was first introduced in Equation (7), can be rewritten as:

$$\sigma_{od} = \sigma_o(\bar{\varepsilon}_p)\left\{1 + 0.0279\left(\frac{\dot{\varepsilon}}{10^{-5}}\right)^{0.3302}\right\} \tag{13}$$

in which σ_{od} is now a yield function both of the strain history and the current strain rate $\dot{\varepsilon}$. The reader is referred to the work of Liu (1985) for a detailed explanation of this consideration. Otherwise, because the cracking tensile strain of concrete is almost invariable in dynamic loading, the cracking is governed by a maximum tensile strain criterion. Then, the response of concrete under tensile stresses is assumed to be linear elastic until the fracture surface is reached (see Figure 2a) and then, its behavior is characterized by an orthotropic material. Cracks are assumed to occur in planes perpendicular to the direction of the maximum tensile strain as soon as this strain reaches the specified concrete tensile strain ε_{ct}. After cracking has occurred the elastic modulus and Poisson's ratio are assumed to be zero in the perpendicular direction to the cracked plane, and a reduced shear modulus is employed. Due to bond effects, cracked concrete carries, between cracks, a certain amount of tensile force normal to the cracked plane. This effect is considered through a relationship between the strain and the stress normal to the cracking plane direction, as shown in Figure 3a.

In Figure 3a f_t is the maximum tensile stress associated to the tensile strain ε_{ct} and the normal stress σ_j is determined from the current strain ε_j as established in the following expression:

$$\sigma = f_t e^{\frac{-(\varepsilon_j - \varepsilon_{ct})}{\alpha}} \tag{14}$$

where α is a softening parameter obtained from the concept of fracture energy of concrete G_f. The use of the fracture energy guarantees that the numerical response will be independent of the finite element mesh (Cervera et al., 1988). The steel reinforcement is modeled as an one-dimensional elasto-plastic material with a constant elastic modulus E_s and a tangential modulus $E_{s'}$ according to the bilinear stress-strain relation shown in Figure 3b. This relation is the same for tension and compression stresses and hysteretic loops are allowed to be formed. The interested reader is referred to the work of Tamayo et al. (2012) for more details about this constitutive model.

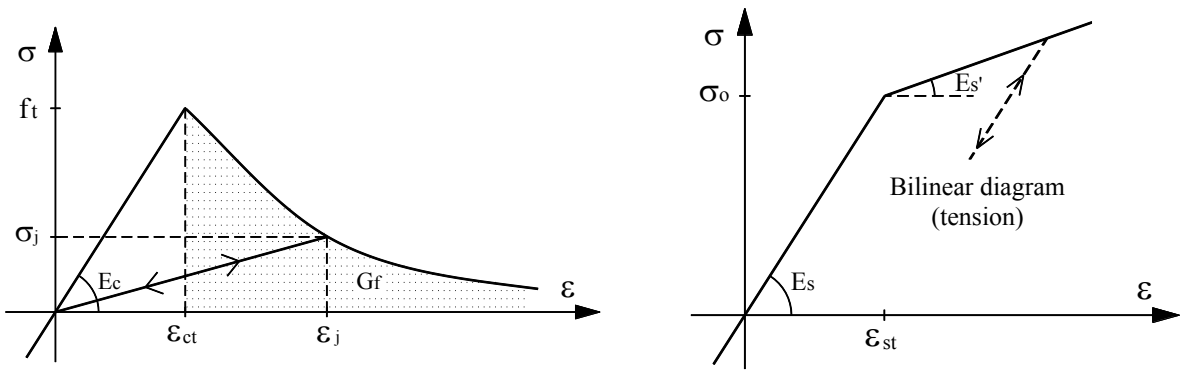

Figure 3: a) Tension stiffening model b) Constitutive law for steel

3 NUMERICAL ALGORITHM

In order to introduce the implicit numerical algorithm for the solution of the nonlinear dynamic equation, it is necessary to describe the predictor and corrector form of the Newmark scheme for the integration of the semi-discrete system of governing equations. Typically at time station t_{n+1} these equations take the following form:

$$[M]\{a\}_{n+1} + [C]\{v\}_{n+1} + \int [B]^T \{\sigma\}_{n+1}(d_{n+1})d\Omega = f_{N+1} \tag{15}$$

where $[M]$ and $[C]$ are the mass and damping matrices, respectively while $\{a\}_{n+1}, \{v\}_{n+1}$ and $\{d\}_{n+1}$ are the acceleration, velocity and displacement vectors, respectively. The tangential stiffness matrix $[K]_{et}$ is related to the internal forces in the following manner:

$$[K]_{et}\{\Delta d\}_n = \int [B]^T \{\sigma\}_{n+1}(d_{n+1})d\Omega - \int [B]^T \{\sigma\}_n(d_n)d\Omega \tag{16}$$

with

$$K_{et} = \int [B]^T [D]_{ep} [B] d\Omega \tag{17}$$

In the Newmark scheme the displacement and velocity at time t_{n+1} can be expressed in the following form:

$$\{d\}_{n+1} = \{\widetilde{d}\}_{n+1} + \Delta t^2 \beta \{a\}_{n+1} \tag{18}$$

$$\{v\}_{n+1} = \{\widetilde{v}\}_{n+1} + \Delta t \gamma \{a\}_{n+1} \tag{19}$$

with

$$\{\widetilde{d}\}_{n+1} = \{d\}_n + \Delta t\{v\}_n + \Delta t^2 (1/2 - \beta)\{a\}_{n+1} \tag{20}$$

$$\{\widetilde{v}\}_{n+1} = \{v\}_n + \Delta t(1-\gamma)\{a\}_n \tag{21}$$

Note that $\{d\}_n, \{d\}_{n+1}$ and $\{d\}_{n+1}$ are the approximations to $d(t_n)$, $\dot{d}(t_n)$ and $\ddot{d}(t_n)$ and β and γ are free parameters which control the accuracy and stability of the method. $\{\widetilde{d}\}_{n+1}$ and $\{\widetilde{v}\}_{n+1}$ are the predictor values and $\{d\}_{n+1}$ and $\{v\}_{n+1}$ are the corrector values. Initially the displacements $\{d\}_0$ and velocities $\{v\}_0$ are provided and the acceleration $\{a\}_0$ is obtained from the following expression:

$$[M]\{a\}_0 = f_0 - [C]\{v\}_0 - [K]_e\{d\}_0 \tag{22}$$

By using Equation (15) to Equation (21), an effective static problem is formed which is solved using a Newton Raphson scheme. This algorithm is summarized in the following manner:

1. Set iteration counter $i = 0$
2. Begin predictor phase in which we set

$$\{d\}_{n+1}^i = \{\widetilde{d}\}_{n+1} = \{d\}_n \tag{23}$$

$$\{v\}_{n+1}^i = \{\widetilde{v}\}_{n+1} = \{v\}_n \tag{24}$$

$$\{a\}_{n+1}^{i} = \left(\{d\}_{n+1}^{i} - \{\tilde{d}\}_{n+1}\right)/(\Delta t^2 \beta) \tag{25}$$

3. Evaluate residual forces

$$\{\psi\}^{i} = \{f\}_{n+1} - [M]\{a\}_{n+1}^{i} - [C]\{v\}_{n+1}^{i} - \int [B]^T \{\sigma\}_{n+1}^{i}\left(\{d\}_{n+1}^{i}\right)d\Omega \tag{26}$$

4. If required, form the effective stiffness matrix using the expression:

$$[K]^{*} = [M]/(\Delta t^2 \beta) + \gamma[C]_T/(\Delta t\beta) + [K]_T(d_{n+1}^{i}) \tag{27}$$

5. Factorize, forward reduction and back substitute as required to solve

$$[K]^{*}.\{\Delta d\}^{i} = \{\psi\}^{i} \tag{28}$$

6. Enter corrector phase in which we set

$$\{d\}_{n+1}^{i+1} = \{d\}_{n+1}^{i} + \{\Delta d\}^{i} \tag{29}$$

$$\{a\}_{n+1}^{i+1} = \left(\{d\}_{n+1}^{i} - \{\tilde{d}\}_{n+1}\right)/\left(\Delta t^2 \beta\right) \tag{30}$$

$$\{v\}_{n+1}^{i+1} = \{v\}_{n} + \Delta t\gamma\{a\}_{n+1}^{i+1} \tag{31}$$

7. If Δd^i and/or ψ^i do not satisfy the convergence conditions then set $i = i+1$ and go to step 3, Otherwise continue. Set

$$\{d\}_{n+1} = \{d\}_{n+1}^{i+1} \tag{32}$$

$$\{v\}_{n+1} = \{v\}_{n+1}^{i+1} \tag{33}$$

$$\{a\}_{n+1} = \{a\}_{n+1}^{i+1} \tag{34}$$

8. Set n = n+1, form $Cv_{n+1} + \int B^T \sigma_{n+1}(d_{n+1})d\Omega$ and begin the next time step.

In this work, the containment shell is subjected to the action of the horizontal components of acceleration of an earthquake. The cost of a time history analysis increases linearly with the accelerogram duration. This has motivated the development of short duration accelerograms which are in some sense compatible with the design response spectrum. Here, the Johnson-Epstein sinesweep analytical earthquake will be used as a prescribed horizontal acceleration history. A maximum acceleration level of 0.33g is prescribed. The sinesweep accelerogram which is equivalent to the El Centro accelerogram is shown in Figure 4 and its values are defined as:

$$\ddot{d}_g(t) = \ddot{d}_{\max}^{g}(\omega)\left[\sin(\theta(t)\right] \tag{35}$$

where

$$\omega = \dot{\theta}(t)/2\pi \tag{36}$$

$$\theta(t) = At + Bt^N \tag{37}$$

$$\ddot{d}^g_{\max} = 0.22\omega.g \quad \omega < 1.5 \tag{38}$$

$$\ddot{d}^g_{\max} = 0.33.g \quad 1.5 < \omega < 3.5 \tag{39}$$

$$\ddot{d}^g_{\max} = 2.16/\varpi^{1.5}.g \quad 3.5 < \omega \tag{40}$$

where, $\ddot{d}_g(t)$ is the ground acceleration time history, $\ddot{d}^g_{\max}$ is the maximum ground acceleration as a function of specific forcing frequency ω, g is the acceleration due to gravity and $\sin(\theta(t)$ is the variable frequency sinusoidal signal. The free parameters are defined as A=1.0, B=3.0 and N=3.0. When the containment shell is subjected to the earthquake acceleration, the generalized force on the right hand side of equation (26) is defined in the following manner:

$$\{f\}_{n+1} = -[M]\{I\}\ddot{d}_g(t) \tag{41}$$

where $[M]$ is the mass matrix and $\{I\}$ is a vector indicating the direction of the earthquake excitation.

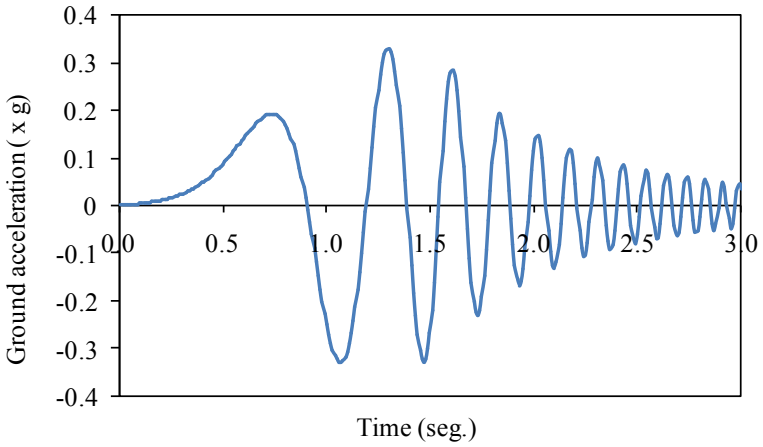

Figure 4: Sine sweep earthquake

4 NUMERICAL EXAMPLE

4.1 Non-linear dynamic response of the reinforced concrete containment shell

The numerical model was used to carry out studies on the nonlinear dynamic response of an RC nuclear containment shell subjected to seismic excitation defined by the sine sweep earthquake function, previously shown in Figure 4. The geometry and the reinforcement details of the containment shell are shown in Figure 5 and the corresponding finite element mesh is shown in Figure 6. Material properties are listed in Table 1.

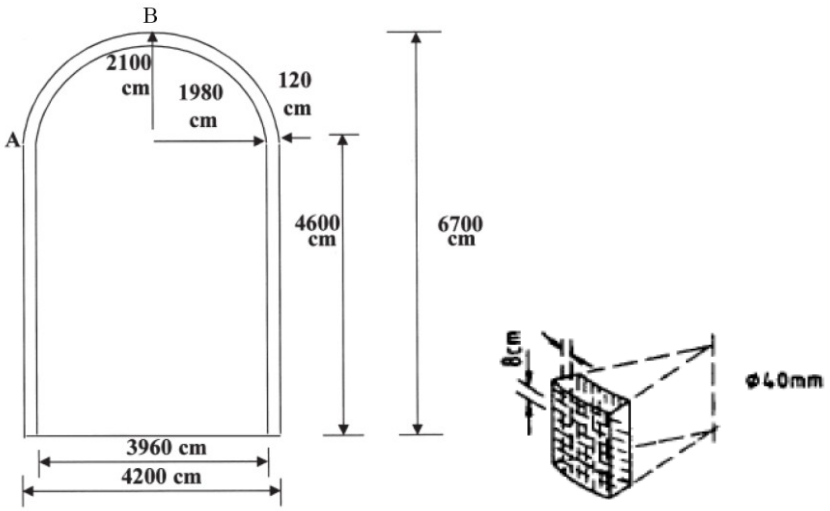

Figure 5: Geometry of reinforced concrete nuclear containment shell adapted from Manjuprasad et al. (2001)

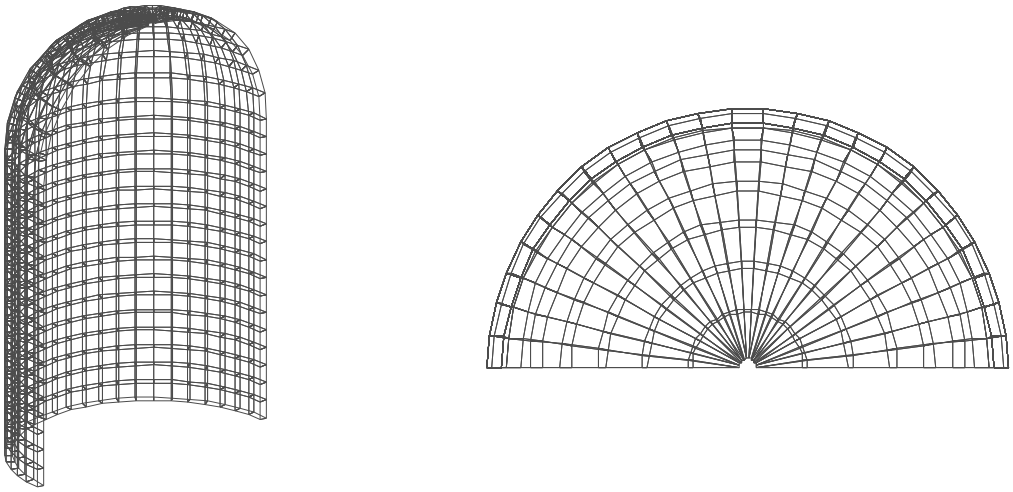

Figure 6: Nuclear containment structure under seismic loading: Finite element mesh

Material Properties (cm,Kg)					
Concrete			Steel		
Elastic modulus	E_c =	300000	Elastic modulus	E_s =	2100000
Poisson	υ =	0.17	Hardening	$E_{s'}$ =	0
Ultimate compressive strength	f_c =	350	Yield stress	σ_o =	4600
Ultimate tensile strain	ε_t =	0.00018			
Ultimate compressive strain	ε_u =	0.0035			
Fracture energy	G_F =	0.2			

Table1: Material Properties.

This built-in reinforced concrete shell was studied earlier by Tamayo et al. (2013) under aircraft impact load. It is composed of cylindrical and spherical parts of constant thickness. The reinforcement, placed circumferentially and meridionally on the interior and exterior surfaces, consisted of bars of diameter 40 mm, spaced at 80 mm. A mesh of 650 20-noded

solid elements was used here (see Figure 6). For non-linear problems of reinforced concrete structures, the ratio of elastic fundamental period of vibration to the time step of integration (Δt), i.e. $T/\Delta t$ should be between 20 and 30 to keep the computational errors within acceptable limits. The elastic fundamental period of vibration (T) of the shell is 0.23 s. A time step of $\Delta t = 0.01$ (T/23) with a total of 1020 steps was used for time step integration phase. The implicit Newmark algorithm with $\beta = 0.25$ and $\gamma = 0.50$ is used. Firstly, a linear elastic analysis is performed. Figure 7 compares the horizontal displacement-time curves for point A obtained in the present work with those obtained in Liu (1985) where shell finite elements were used. Similar results for the same point are shown in Figure 8, but now for the nonlinear case where an ultimate concrete cracking strain of 0.00018 was defined. Comparisons of linear and nonlinear responses obtained in the present work are shown in Figure 9. As it can be seen in all these figures, presents results compared well with those obtained in Liu (1985).

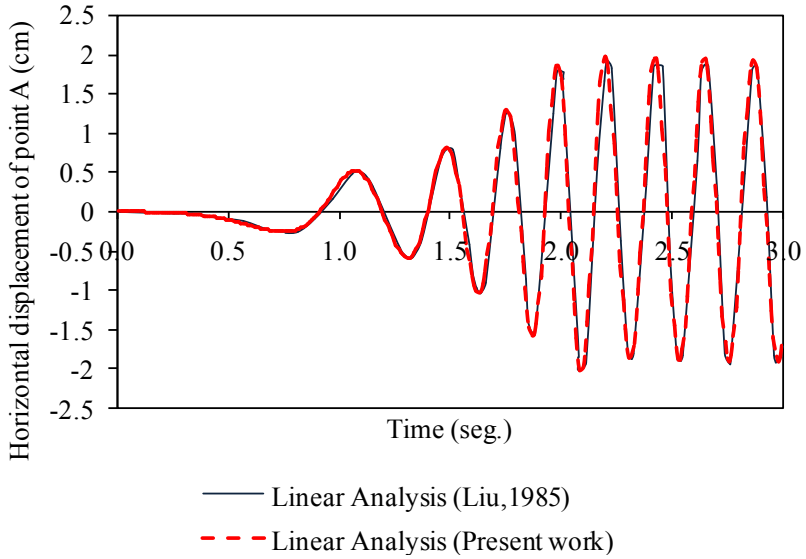

Figure 7: Nuclear containment structure under seismic loading: Linear response at point A

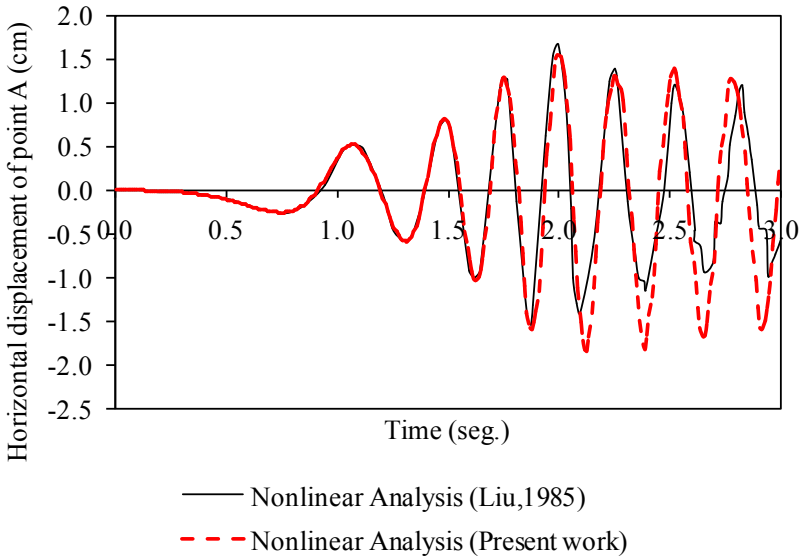

Figure 8: Nuclear containment structure under seismic loading: Nonlinear response at point A

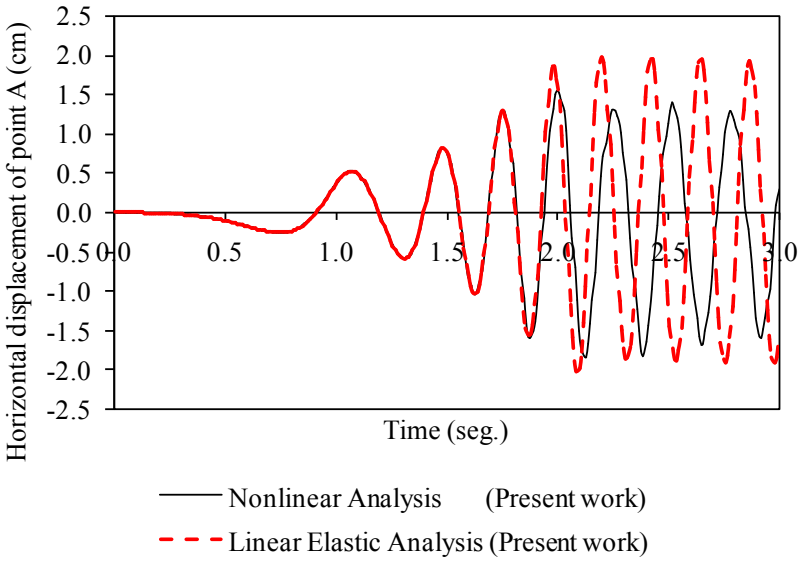

Figure 9: Nuclear containment structure under seismic loading: Comparison of linear and nonlinear response at point A

In Figure 10 and Figure 11 are shown the horizontal displacement-time curves for point B for the linear and nonlinear cases, respectively. As it can be seen, present results also compare well with those obtained in Liu (1985). Comparisons of linear and nonlinear responses obtained in the present work for this point are depicted in Figure 12.

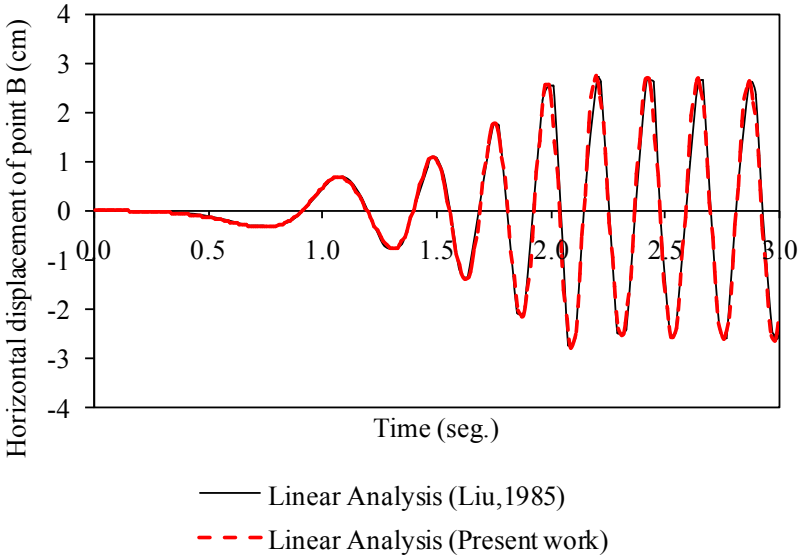

Figure 10: Nuclear containment structure under seismic loading: Linear response at point B

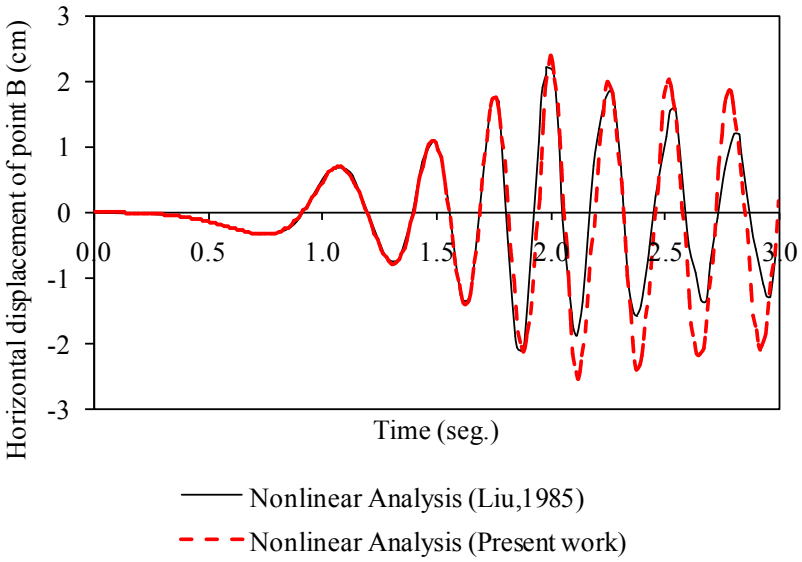

Figure 11: Nuclear containment structure under seismic loading: Nonlinear response at point B

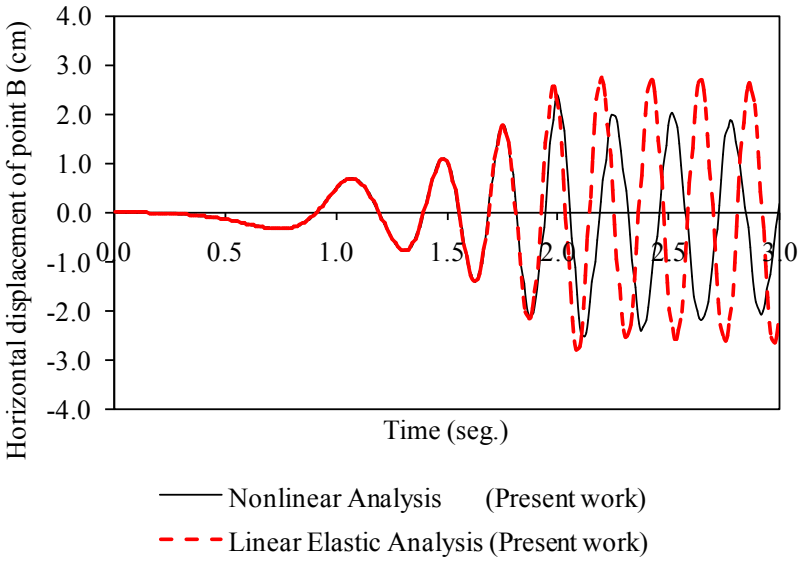

Figure 12: Nuclear containment structure under seismic loading: Comparison of linear and nonlinear response at point B

Finally, in Figure 13 is shown the spreading of the cracks obtained with the present numerical model for the nonlinear analysis performed for different times of analysis. In Figure 14, the crack patterns obtained in Cervera et al. (1988), where only 40 20-noded solid finite elements were used, are also shown. As it is shown, both numerical models predict the progressively development of cracking from the left to the right side at the base of the nuclear containment.

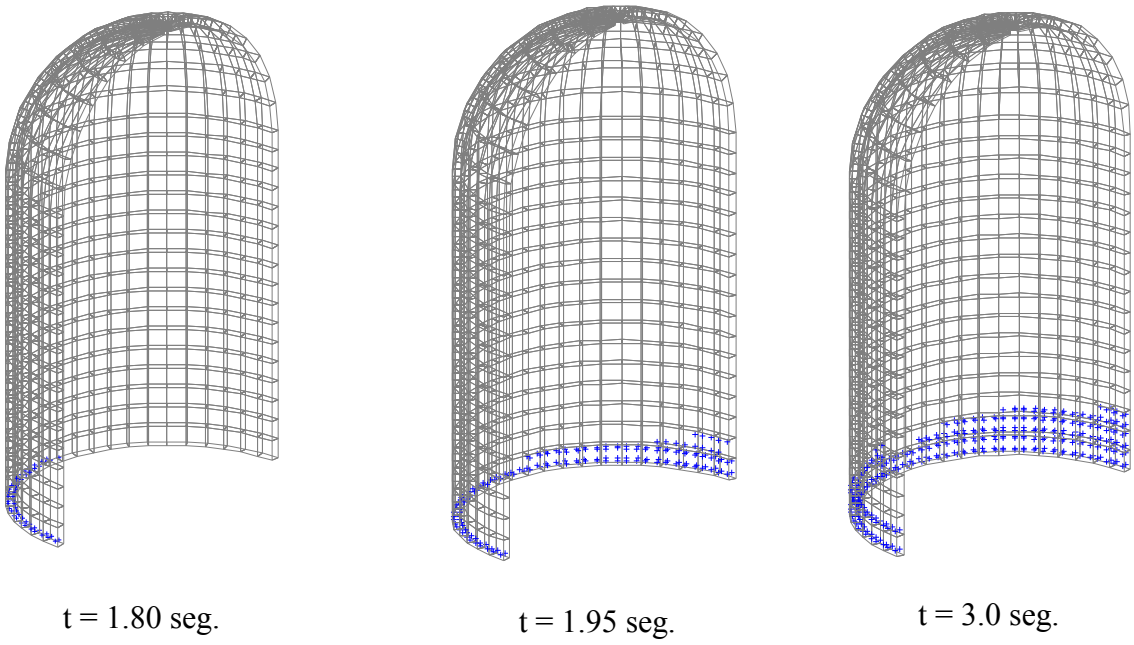

Figure 13: Crack patterns at different times for concrete with a cracking strain of 0.00018 (Present work)

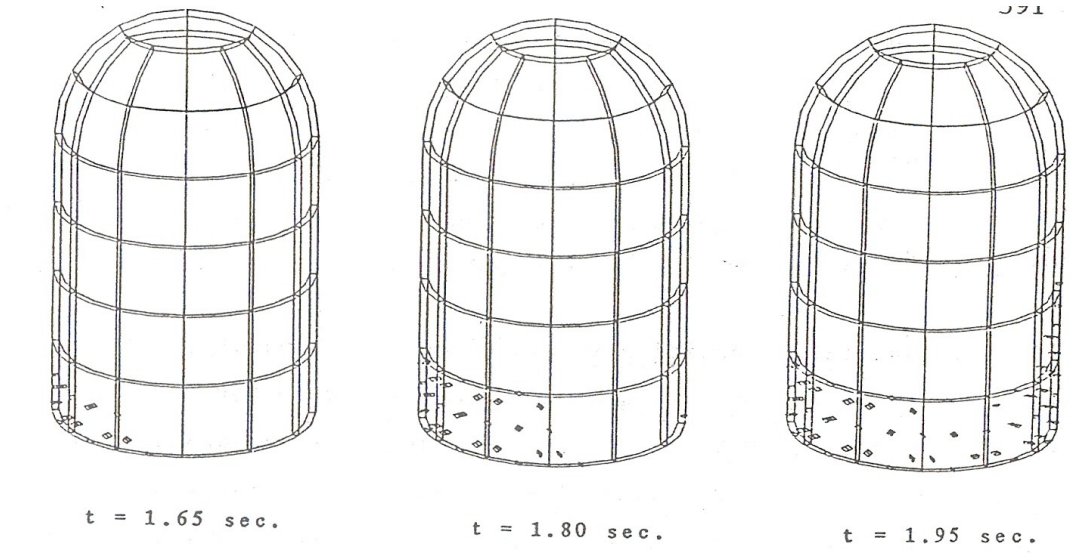

Figure 14: Crack patterns at different times for concrete with a cracking strain of 0.00018 (Cervera et al. 1988)

5 CONCLUSIONS

In this work, a three-dimensional numerical model for the nonlinear dynamic analysis of a reinforced concrete containment shell under seismic load is presented. A 20-noded brick finite element is used to model the concrete part whereas reinforcing steel bars are modeled using incorporated membrane elements. The present example was previously analyzed by other

authors under aircraft impact (see e.g. Tamayo, 2013). Time-displacement histories for two different points on the shell were monitored when both linear and nonlinear analysis are performed. Validation of the model for seismic load was done by comparing present results with those obtained by Liu (1985) in relation of time history displacements and with those obtained by Cervera et al. (1988) for cracking patterns.

As it can be seen from the time history curves for both studied points, the period of vibration is elongated and some dissipation due to nonlinear effects is evident. Also, the amplitude is smaller in the nonlinear analysis than in the linear case. Cracking affects the stiffness of the structure, thus changing its fundamental period. The response to a seismic excitation is greatly dependent on the dynamic characteristics of the structure, as the energy absorbed by the system depends both on the forcing and the natural frequencies.

6 ACKNOWLEDGEMENT

The authors gratefully acknowledged the financial support provided by CAPES and CNPQ.

REFERENCES

Cervera M., Hinton E., Bonet J. and Bicanic N. *Nonlinear transient dynamic analysis of three dimensional structures – A Finite element program for steel and reinforced concrete materials*. Numerical Methods and Software for Dynamic Analysis of Plates and Shells. Pineridge Press, 1988. p320-504.

Liu G. Q., *Nonlinear and transient finite element analysis of general reinforced concrete plates and shells*, 1985. PhD Thesis. Department of Civil Engineering, University College of Swansea. Swansea, UK.

Manjuprasad, M., Gopalakrishnan, S., and Appa Rao T.V.S.R., Non-linear dynamic response of a reinforced concrete secondary containment shell subjected to seismic load. *Engineering Structures*, 23:397–406, 2001.

Tamayo, J.L.P., Awruch A.M. and Morsch, I.B. Dynamic Analysis of Reinforced Concrete Structures. *Tecnia (Lima)*, 26:33–42, 2012.

Tamayo, J.L.P., Morsch, I.B., e Awruch A.M., Static and dynamic analysis of reinforced concrete shells. *Latin American Journal of Solids and Structures*, 10:1109–1134, 2013.

Tamayo, J.L.P., Morsch, I.B., e Awruch A.M., Numerical modeling of reinforced concrete structures: Static and Dynamic Analysis. *REM Revista Escola de Minas.*, accepted for publication 2013.